Dynamic Model and Converter-Based Emulator of a Data Center Power Distribution System

Jingjing Sun , *Student Member, IEEE*, Shuyao Wang , *Member, IEEE*, Jingxin Wang , *Member, IEEE*, and Leon M. Tolbert , *Fellow, IEEE*

Abstract—Data centers have become a widespread power electronics (PE) load, which has significant impact on the power grid. In order to investigate the data center load characteristics, this article proposes a complete dynamic model for a typical data center ac power distribution system. A generalized model with mode transition is proposed to coordinate different power stages in the data center power system. Meanwhile, to help evaluate the grid dynamic performance and transient stability, an all-in-one load data center power emulator is developed on a reconfigurable PE converter-based hardware testbed (HTB). The dynamic power model is digitized and simplified to be implemented in two local voltage source inverters on the HTB. This proposed data center power emulator has been verified experimentally in a regional network. Dynamic performances during voltage sag events and server load variations are emulated and discussed. The article details the design, development, and verification of the data center model and power emulator. The proposed model and emulator provide an effective, easy-to-use tool to better design data centers and study the interaction with the power system.

Index Terms—Data center, dynamic model, hardware testbed (HTB), power distribution, power emulator, server load, voltage sag.

I. INTRODUCTION

A. Background

DATA centers are dedicated to collecting, storing, processing, and distributing large amounts of data, which are indispensable for today's computing and networking society. Over the past two decades, data centers have been constructed around the world, leading to a considerable power consumption [1]. The global electricity demand by data centers has increased from 153 TWh in 2005 to 205 TWh in 2018, accounting for almost 1% of the total electricity supply in the world [2].

Apart from a large energy consumer, a data center is also a complicated system with a high density of power electronics (PE) and controls [3]. As shown in Fig. 1, a typical data center
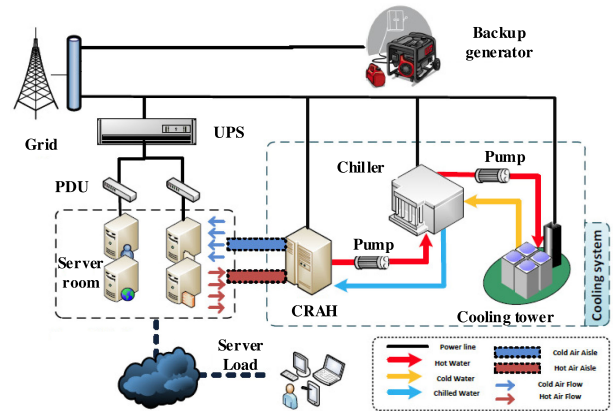
Fig. 1. Internal structure of a typical data center [3].

is composed of a power supply system, cooling system, backup energy, lighting system, server loads, etc., which contain multiple PE converters. Also, the control strategy is complex to enable reconfigurable structures and multiple operation modes [4].

B. Motivation

1) Lack of Complete Dynamic Data Center Power Model: As a large electric load with high penetration and nonlinear performance, data center's influence on the power grid is significant. Meanwhile, to evaluate the grid voltage stability and transient stability (TS) performance, the accuracy of the power load model has been emphasized, and efforts have been made to develop effective dynamic load models [5], [6]. Compared with the conventional load model in TS programs, the data center load has distinct characteristics. On the one hand, data centers exhibit dynamic server load profile, which results in apparent power demand fluctuations in a short time [7]. On the other hand, grid disturbances/contingencies, such as a voltage sag event, would result in a reconfigured structure and operation mode transition within the data center, leading to dynamic response on the power grid [4]. Therefore, it is important to investigate the data center load characteristics, and a complete and accurate dynamic power model is required.

Researchers have developed a number of data center power models, which can be generally divided into four categories. The first kind of model focuses on one or two aspects of the data center that is of interest for the research, *e.g.,* model of one server load (CPU) [8], model of one cooling component [9],

etc. Though detailed, these models are incomplete to reflect the overall performance of the data center. The second type of model is based on mathematical calculation of the whole system [7], [10]. A coherent data center power model is proposed in [10] that covers complete facilities, including the cooling system, electrical infrastructure, server room, and server loads. This model is complete to capture the static operation, but it cannot predict dynamic performances during transient conditions because it lacks detailed circuit modeling.

The third group of models is data driven, where some parameters are supplied by prerecorded data from a given data center [11], [12]. Such models are highly dependent on the provided data, which are usually not openly available. The last category builds models of various power components for dynamic simulation of the data center [13], [14]. Nevertheless, the established models are oversimplified and inaccurate, e.g., using RLC load to represent the server load or cooling load, and converters' closed-loop controls are not considered. Therefore, there is a lack of data center power load model that is complete and accurate to reflect the dynamic load performance.

2) Lack of Converter-Based Data Center Power Emulator: The data center model is typically implemented in a simulation or emulation platform to explore the load characteristic and grid dynamic performance. Digital simulation tools, including PSS/E, TSAT, PSCAD, MATLAB/Simulink, and Saber, can be used for studying different types of power circuits [15]. Real-time digital simulators combine the digital simulation and physical test together to form a hardware-in-the-loop emulation [16]. Analog-based emulation is another area, where hardware-based testbeds or down-scaled prototypes have been developed to verify the proposed devices or controllers [5], [17].

Compared with analog-based emulators, digital-based simulators/emulators are relatively cheaper, smaller, and easy to be installed or modified. However, digital simulation/emulation suffers from instability and convergence issues, and tends to ignore realistic conditions, such as sensing errors, communication time delay, control bandwidth, and switching noise [18], [19]. Although analog-based emulators are usually more expensive, heavier, and less accessible, the testing results are more convincing and preferred by most engineers [17].

In [5], a unique hardware testbed (HTB) platform is developed in the NSF/DOE Engineering Research Center, CURENT, to overcome the issues with digital simulators and conventional analog emulators. The HTB is a multiconverter-based reconfigurable real-time grid emulator, which is used to perform real power tests and emulate the power grid with broad time scales (μs to s), reduced computational resources, and capability of emulating precise transient response. By programming the interconnected three-phase voltage source inverters (VSIs), many different power elements can be emulated [20]. Based on the HTB, load emulators that have been developed include ZIP load [5], induction motor load [21], variable frequency drive (VFD)-based load [22], and battery energy storage system [23]. However, none of them can reflect the data center dynamic performance. Hence, it is critical to create a data center power load emulator to carry out the related grid experiments for evaluating the grid dynamic performance and TS.

C. Contributions

This article concentrates on modeling and emulation of the data center power distribution system, to investigate data center load characteristics and improve the accuracy of power grid dynamic evaluation. The main contributions include the following.

1) A complete and accurate data center power system dynamic model is proposed, which is consistent with the current data center market and able to predict data center dynamic power performance in different operation modes.
2) A generalized model with a top-level control is proposed to coordinate different power stages and predict the data center load characteristics in different operation modes.
3) A converter-based data center power emulator is developed based on the CURENT HTB, which is capable of demonstrating versatile power tests during transient conditions, such as load variation and voltage sag.
4) Digitized dynamic power model and reasonable simplification are proposed to implement the data center power emulator as an all-in-one load, making the data center power emulator a flexible and easy-to-use tool for performing various grid experiments.

The article is an extension of the work in [24], and the rest of this article is organized as follows. Section II investigates the typical data center system circuit and operation principle. Section III illustrates the proposed data center dynamic power model. Section IV presents the strategy of developing the data center power emulator. Section V shows the experimental verification of the data center power emulator. Finally, Section VI contains the discussion and concludes this article.

II. DATA CENTER CIRCUIT AND OPERATION PRINCIPLE

A. Circuit Topology and Control

Fig. 2 shows the widely-used data center ac power distribution system with centralized uninterrupted power supply (UPS) and air cooling [4]. The power supply system consists of the UPS, power distribution units (PDUs), power supply units (PSUs), and motherboards for server loads. The UPS is used to condition and compensate the input ac power during grid disturbances so that stable power is ensured for server loads. The cooling system is primarily composed of a cooling tower, chiller, water pumps, computer room air handler (CRAH), and distributed server fans in rack cabinets. Grid-connected induction motors can be used to represent the cooling tower, chiller and water pumps, and the CRAH is represented by a VFD-based motor. Distributed server fans are powered by the dc voltage from PSUs, and are considered as part of the electric load in the power supply system.

In order to practically demonstrate a data center system, commonly used circuit topologies and control strategies for each power component are investigated [25]–[28]. Table II summarizes the adopted circuits and control methods.

B. Operation Principle

The principal task of the data center is to maintain reliable server operation regardless of grid disturbances or a power outage. In order to achieve this and improve the system power
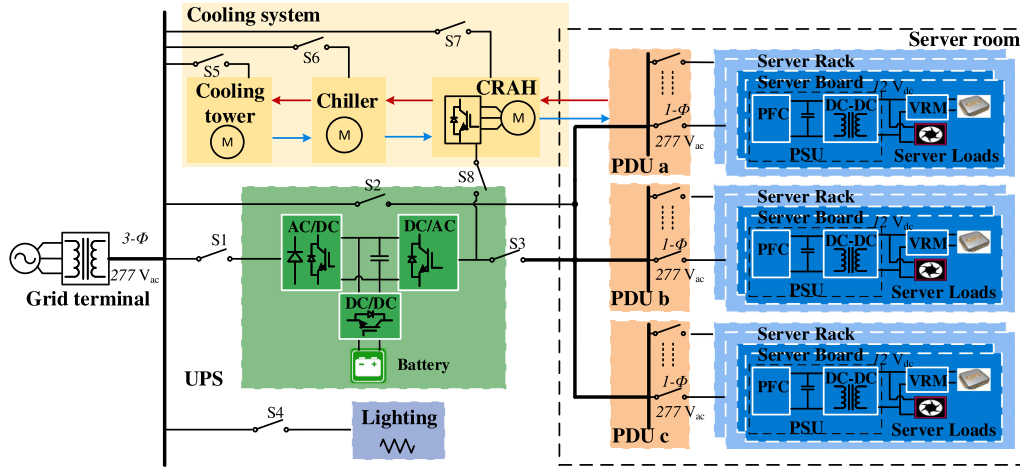
Fig. 2.   Typical structure of a data center ac power distribution system.

TABLE I
DATA CENTER OPERATION MODES IN DIFFERENT VOLTAGE LEVELS

No.	Operation mode	$V_{t,pu}$	$t_{transition}$	S_1	S_2	S_3	S_4	S_5	S_6	S_7	S_8
0	Normal eco mode	0.9 - 1.1	N/A	ON	ON	OFF	ON	ON	ON	ON	OFF
1	Double conversion mode	0.7 - 0.9	500 ms	ON	OFF	ON	ON	ON	ON	ON	OFF
2	Battery mode	≤ 0.7	20 ms	OFF	OFF	ON	ON	OFF	OFF	OFF	ON

usage effectiveness, data centers are normally implemented with multimode operation, which is realized by reconfigurable structures and controls [33]. In this article, three widely-used operation modes are employed.

1) *Normal eco mode*: When the utility power is within acceptable limits, the UPS is bypassed, and the server loads are directly supported by the utility power through PDUs and PSUs. To achieve seamless transition and reduce the start-up delay when power failure occurs, the UPS is turned ON and operates at light load (i.e., 1% load).

2) *Double conversion mode*: When the utility voltage is not within the data center allowed range but still within the UPS input range, the UPS switches into double conversion mode. Server loads are directly fed by the regulated power from the UPS and are not influenced by grid disturbances.

3) *Battery mode*: When power failure or severe grid interruption occurs, the UPS is disconnected from the grid and switches into battery mode, where the backup battery provides the dc power to the inverter. Server loads are continually supplied by the UPS until utility power is restored or an alternative power source comes online.

During severe power disruption, the cooling system including the cooling tower, chiller, water pumps, and the CRAH are disconnected from the grid [34]. To maintain the air circulation and keep the server room temperature within an acceptable range, CRAH is powered by the UPS backup power until the ac source is restored.

On the other hand, input power of the information technology equipment should remain in the safe area as stipulated in the information technology industry council (ITIC), which means the operation mode transition time must be less than the allowed power downtime [35]. Considering the ITIC standard and commercial applications, an operation principle in response to different voltage levels are identified, as presented in Table I, where S_1–S_8 correspond to switches shown in Fig. 2, and $t_{\text{transition}}$ is the time for the system to change the operation mode after a voltage sag occurs, i.e., data center switches into double conversion mode 500 ms after $V_{t,\text{pu}}$ decreases below 0.9, and switches into battery mode 20 ms after $V_{t,\text{pu}}$ decreases below 0.7.

III. PROPOSED DATA CENTER DYNAMIC POWER MODEL

In this section, a complete dynamic power model of the data center power distribution system is proposed.

A. Detailed Power Converter Modeling

The main power converters in the data center power distribution system include UPS, PSU, CRAH VFD, and cooling motors. Fig. 3 shows the circuit topologies of the UPS, PSU, and VFD-based motor. Because this model is for investigating line-cycle dynamic performance on the grid, an average model that neglects switching ripple is accurate enough to model the data center power converters. Closed-loop controls are implemented, and all controller parameters are designed under a per unit (p.u.) system so that the system can be scaled flexibly with different power ratings without rebuilding the controllers.

1) UPS Model: As shown in Fig. 3(a), the UPS contains a front-end rectifier, a VSI, a dc–dc converter, and an energy storage system with battery pack. In continuous conduction mode (CCM) operation, the average model of the UPS is derived,

TABLE II
WIDELY USED CIRCUIT TOPOLOGIES AND CONTROL METHODS IN DATA
CENTER

UPS front-end rectifier	
Topology	Three-phase boost-type PFC rectifier [29]
Nominal voltages	Three-phase 480/277 V_{ac} - 960 V_{dc}
Control method	Peak current mode control
UPS inverter	
Topology	Three-phase voltage source inverter [30]
Nominal voltages	960 V_{dc} - Three-phase 480/277 V_{ac}
Control method	Dual-loop space vector control
UPS dc-dc stage	
Topology	Half-bridge dc-dc converter
Nominal voltages	600 V_{dc}-960 V_{dc}
Control method	Average current mode control [31]
UPS battery	
Battery type	Lithium-ion battery [25]
Nominal voltage	600 V_{dc}
	2 paralleled battery strings (each with 182 cells)
PSU PFC converter	
Topology	One-phase boost PFC converter [26]
Nominal voltages	One-phase 277 V_{ac} - 480 V_{dc}
Control method	Average current mode control
PSU dc-dc isolated converter	
Topology	Full-bridge LLC converter
Nominal voltages	480 V_{dc} - 48 V_{dc}
Control method	Variable frequency control [27]
CRAH VFD front-end rectifier	
Topology	Three-phase active boost rectifier [30]
Nominal voltages	Three-phase 480/277 V_{ac} - 800 V_{dc}
Control method	Dual-loop space vector control
CRAH VFD inverter	
Topology	Three-phase voltage source inverter
Control method	Constant V/Hz control [32]

Fig. 4. UPS average model.

Fig. 5. Control diagram of the three-phase boost-type PFC rectifier in UPS.

Fig. 6. Control diagram of the three-phase VSI in UPS.

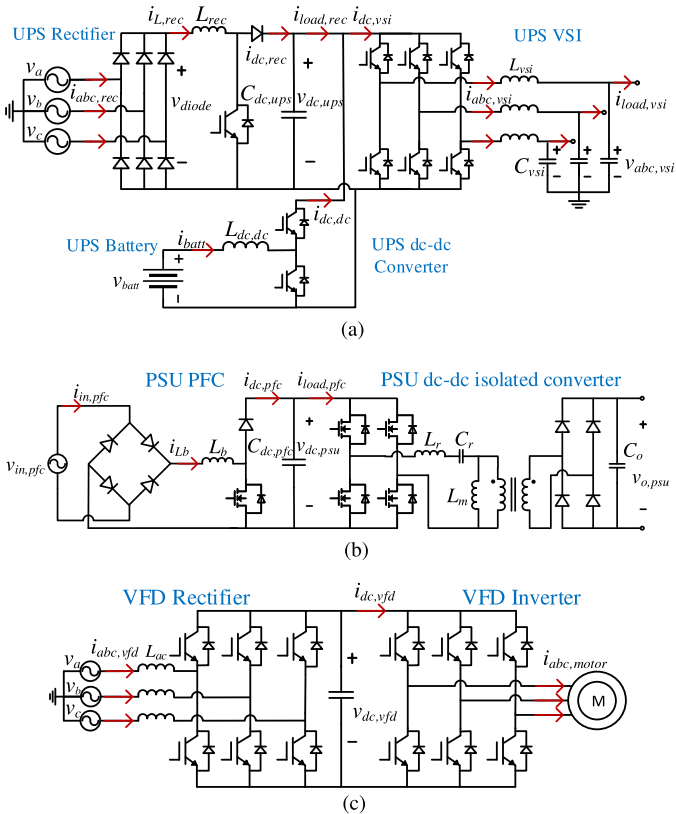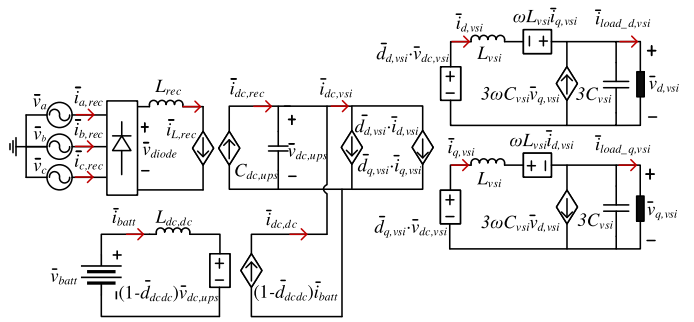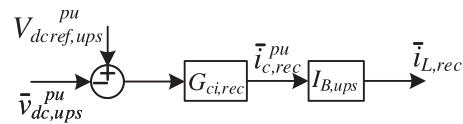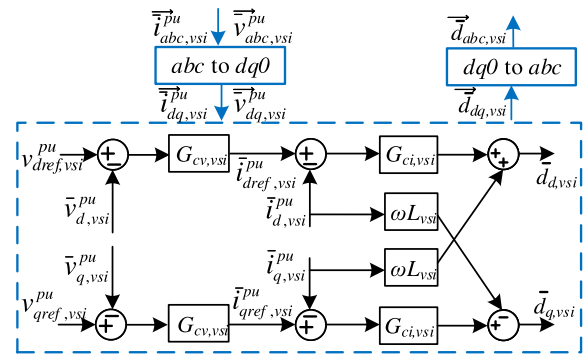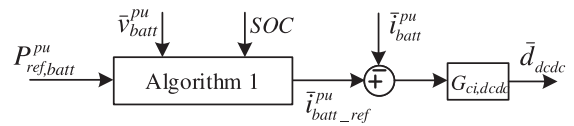Fig. 7. Average current mode control of the dc–dc converter in UPS.

Fig. 3. Circuit topologies of the power converters in the data center system. (a) UPS circuit. (b) PSU circuit. (c) VFD-based motor circuit.

as shown in Fig. 4. A three-phase boost-type PFC rectifier is adopted in the UPS rectifier. Although the input current quality can be improved by certain modulation and control [36], the widely used CCM peak current mode control is employed (see Fig. 5) [37]. An average model in the synchronous direct-quadrature (dq) coordinate system is built for the VSI, and dual-loop space vector control is employed to regulate the VSI voltage and power [30], as illustrated in Fig. 6.

A bidirectional half-bridge dc–dc converter is used for the UPS energy storage system with average current mode control. During the normal eco mode and double conversion mode, the UPS dc-link voltage $v_{dc,ups}$ is regulated by the rectifier, and the dc–dc converter is responsible for charging or discharging the battery. As elaborated in Fig. 7, the inductor average
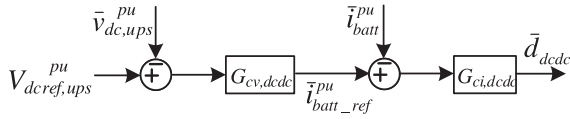
Fig. 8. Dual-loop control of the dc–dc converter during battery mode.

Algorithm 1: Battery Charging and Discharging.

Input:
$P^{pu}_{ref,batt}$: battery active power reference in pu;
$\bar{v}^{pu}_{batt}$: battery pack terminal voltage in pu;
SOC : battery SOC;
Output:
$\bar{i}^{pu}_{batt\_ref}$: current reference for dc-dc converter in pu;
Procedure:
if $P^{pu}_{ref,batt} > 0$ **then**
   if $SOC > SOC_{min}$ **then**
      $\bar{i}^{pu}_{batt\_ref} = P^{pu}_{ref,batt} \div v^{pu}_{batt}$;   // battery is discharged
   else
      $\bar{i}^{pu}_{batt\_ref} = 0$;
else if $P_{ref,batt} < 0$ **then**
   if $SOC < SOC_{max}$ **then**
      $\bar{i}^{pu}_{batt\_ref} = P^{pu}_{ref,batt} \div \bar{v}^{pu}_{batt}$;   // battery is charged
   else
      $\bar{i}^{pu}_{batt\_ref} = 0$;
else
   $\bar{i}^{pu}_{batt\_ref} = 0$;   // battery stands by

---

current reference is determined by a charging/discharging algorithm (Algorithm 1). To avoid over charging or discharging the battery, the state-of-charge (SOC) minimum limit is set to 20% and maximum limit at 98%. When the system operates in battery mode, the rectifier is OFF, and the dc–dc converter needs to also regulate $v_{dc,ups}$ with an outer voltage loop, as shown in Fig. 8.

The UPS battery pack is composed of paralleled battery strings of Li-ion battery cells. The equivalent Li-ion battery circuit and mathematical equations used in [38] are adopted to model the battery's charging/discharging performance. With the current controlled by the dc–dc converter, the battery's SOC is calculated based on the coulomb counting method [39], as expressed in

$$SOC_{cell} = SOC_0 - \frac{\int_0^t \bar{i}_{cell} dt}{Q_{cell}}. \tag{1}$$

2) PSU Model: The PSU consists of a boost PFC converter and an *LLC* dc–dc isolated converter. The PFC converter improves the power factor and regulates the dc bus voltage. In CCM operation with average current mode control, the PFC average model is presented in Fig. 9(a). Fig. 9(b) shows the control structure of the PFC converter. The outer voltage loop is designed with slow bandwidth (typically < 20Hz) to avoid the influence of the double-line frequency ripple. The inner current loop compensates the average inductor current to achieve unity power factor, and the control bandwidth is much faster.

LLC resonant converter is popular in the isolated dc–dc stage, which has benefits in high-efficiency operation with wide input variation. Variable frequency control with voltage controlled
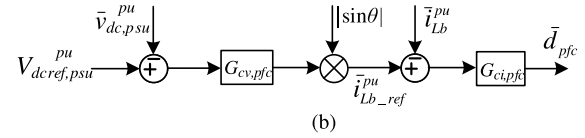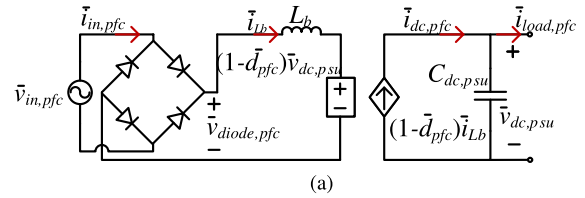

(a)

(b)

Fig. 9. Average model and control diagram of the PSU PFC converter. (a) PFC average model. (b) PFC control diagram.
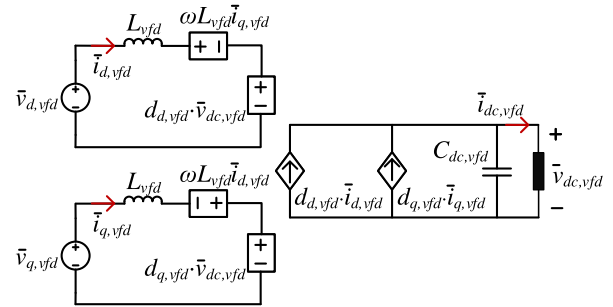

Fig. 10. Average model of the three-phase boost rectifier in dq axis.

oscillator is normally used to regulate the output voltage [27]. Modeling of the *LLC* converter is nontrivial, since the traditional average model is not adaptable for such a high-frequency resonant circuit. Nevertheless, it is not necessary to have the detailed *LLC* model. For present *LLC* converters operating at 50–200 kHZ, the control bandwidth is usually designed at 1–5 kHz. Compared with the PFC slow voltage loop, the dc–dc converter is fully decoupled from the PFC in the control perspective and has little effect on the ac input terminal. In addition, in the low-frequency range within the control loop bandwidth, the *LLC* converter has a negative input impedance and behaves like a constant power load [40]. Therefore, in the model, the isolated dc–dc converter is simplified as a controlled power load depending on the server load.

3) Cooling Motor and VFD Model: Motors are the predominant electrical components in the cooling system. In the model, an aggregated grid-connected induction motor is used to represent the cooling tower, chiller, and water pumps. The dynamic motor model used in [32] is adopted to obtain the transient behaviors.

A two-stage VFD-based motor is adopted for the CRAH, which contains a three-phase active front-end boost rectifier, a VSI, and an induction motor [see Fig. 3(c)]. For the VFD rectifier, the average model is derived in dq coordinates as shown in Fig. 10. Fig. 11 shows the control structure of the rectifier, where the dc bus voltage and the reactive power are regulated in d-axis and q-axis, respectively. The VSI is used to generate
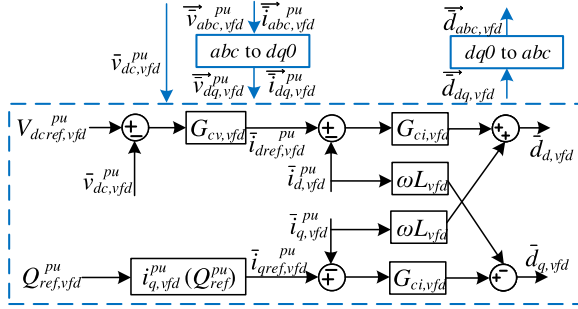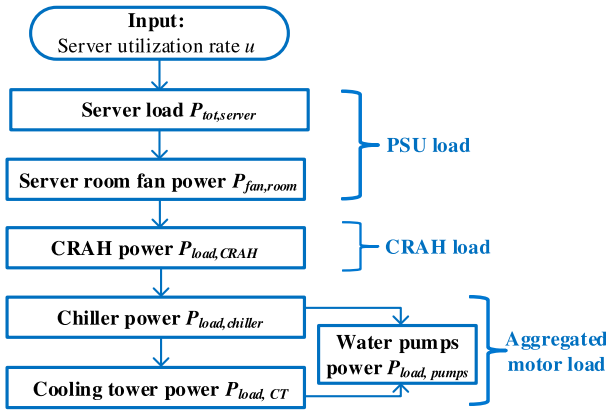
Fig. 11. Control diagram of the three-phase boost rectifier in dq axis.

Fig. 13. Illustration of the generalized model with top-level control.

Fig. 12. Flowchart of the data center server and cooling load model.

flexible ac power and control the motor speed. Advantageous in simplicity and low cost, constant volt-per-hertz (V/Hz) control is employed to drive the induction motor [32].

B. Coherent Server and Cooling Load Model

For the server load modeling, various linear and nonlinear power models have been developed [41], among which the server utilization-based linear power models are popular [3]. In this work, the server power consumption is estimated as

$$P_{\text{server}} = P_{\text{idle}} + (P_{\text{rated}} - P_{\text{idle}})u_{\text{server}} \tag{2}$$

where P_{idle} is the power consumed in idle mode, P_{rated} is the server power rating, and u_{server} stands for the server utilization, which varies from 0% to 100%. Assuming that load balancing is realized, the total server load is predicted as

$$P_{\text{server},tot} = N_{\text{rack}}N_{\text{server}}P_{\text{server}} \tag{3}$$

where N_{rack} and N_{server} represent the number of racks and the number of servers per rack, respectively.

Cooling system modeling is also an active area of research, where different models are developed to estimate the thermal load [9], [10], [42]. In this article, a bottom-up cooling power load model is built. As illustrated in Fig. 12, once server load is calculated based on u_{server}, server fan power consumption can be assessed according to the required air flow. Then, CRAH power load is predicted by the motor rotation speed, which depends on
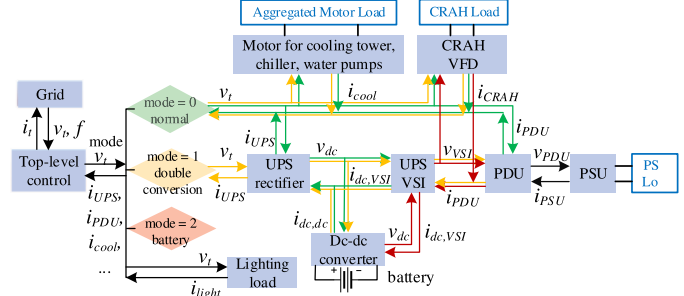
the total air flow in the room outlet and inlet. Next, the hot air from the CRAH is transmitted to the chiller to be cooled down, and the chiller power load is estimated based on the heat from the CRAH and the chiller coefficient of performance (COP). A similar load calculation is also used for the cooling tower, which depends on its thermal load and COP. Meanwhile, power loads of the two water pumps that are used to push the water flow between chiller and cooling tower are calculated based on the water flow rate and water temperature difference. In this way, once u_{server} is given, the power load of each power stage is determined. A detailed calculation of the cooling load is provided in the appendix.

In the typical data center cooling system, dynamic response time of the room temperature regulation is in tens of seconds, depending on the temperature and air velocity sensors and the temperature monitoring time granularity [34], [42]. Therefore, the cooling load dynamic response is slower than the server load variation. In this model, the cooling load dynamic response time is assumed at 10 s, that is the thermal load remains unchanged if server load changes within 10 s but follows the server load variation if it lasts for a longer time.

C. Generalized Model With Mode Transition

One challenge of building the whole data center system model is to coordinate all power stages together and predict the performance in various operation modes. To achieve this, a generalized model with a top-level control for mode transition is proposed in this work, as illustrated in Fig. 13 and Algorithm 2. The model starts with the terminal voltage v_t and grid frequency f, and the top-level control determines the operation mode. Multiple power stages are modeled simultaneously. For each stage's model, the input-port voltage is the output voltage of the previous stage, and the input-port current and output-port voltage are calculated based on the model. The output-port voltage is then sent to the next stage as the input voltage, and the input-port current is sent to the previous stage as the output load current. In different operation modes, voltages and currents are calculated following the specific paths, which are distinguished in different colors in Fig. 13. Finally, the top-level control updates the grid terminal current i_t based on the operation mode and starts the next cycle of calculation.

Algorithm 2: Top-Level Control.

Input:
v_t : grid terminal voltage;
$i_{UPS}, i_{PDU}, i_{cool}$, etc. : currents of different power stages;
Output:
$mode$: system operation mode;
i_t: grid terminal current;
Procedure:
if $v_t > 0.9V_{nom}$ **then**
    if $t_{nom} > 0.25$ s **then**
        | $mode = 0$;   // 0.25 s is the margin time
    else
        | $mode$ is unchanged;
else if $0.7V_{nom} < v_t \le 0.9V_{nom}$ **then**
    if $t_{sag} > 0.5$ s **then**
        | $mode = 1$;
    else
        | $mode$ is unchanged;
else
    if $t_{sag} > 20$ ms **then**
        | $mode = 2$;
    else
        | $mode$ is unchanged;

if $mode = 0$;   // normal eco mode
then
    | $i_t = i_{UPS} + i_{PDU} + i_{cool} + i_{CRAH} + i_{light}$;
if $mode = 1$;   // double conversion mode
then
    | $i_t = i_{UPS} + i_{cool} + i_{CRAH} + i_{light}$;
if $mode = 2$;   // battery mode
then
    | $i_t = i_{light}$;

TABLE III
DEFINED DATA CENTER CONFIGURATION IN SIMULATION

Parameters	Values
Intel Xeon 5500 processor [43]	$P_{idle} = 10$ W
	$P_{rated} = 130$ W
Number of servers per rack, N_{server}	20
Number of racks, N_{rack}	3
Server room $\triangle T_{air,server}$	13.5 °C
Server fan E97379-001 [44]	$P_{rated,fan} = 13.8$ W
CRAH rated power	$P_{rated,CRAH} = 2$ hp
CRAH fan nominal speed	$\omega_{0rm,CRAH} = 188.5$ rad/s
Chiller rated power	$P_{rated,chiller} = 2$ hp
Pump rated power	$P_{rated,pump} = 2$ hp
Cooling tower rated power	$P_{rated,CRAH} = 2$ hp
Chiller water $T_{wcold,chiller}$	16 °C
Cooling tower water $T_{wcold,CT}$	29.44 °C
Water flow rate	$f_w = 8.2 \times 10^{-4}$ m³/s
System power rating	$P_{rated} = 15.068$ kW
UPS Power rating	10 kW
PSU power rating	1.5 kW
Motor inertia	1 s

D. Model Comparison in Simulation

To validate the proposed model, a scaled data center ac power distribution system is defined, as illustrated in Table III. The proposed dynamic model with closed-loop control is built in MATLAB/Simulink. A small power rating is defined in the simulated model, but the data center system can be scaled to a large power rating without changing the control parameters under pu system. To compare with the existing model [13], [14], a conventional data center system model is also built in MATLAB/Simulink, where the server load is represented by a
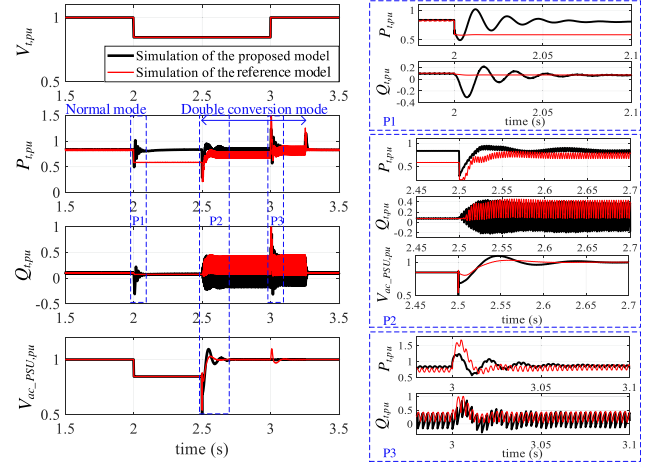

Fig. 14.   Simulation waveforms of the proposed data center model and the reference model in [13] under 16% terminal voltage sag for 1 s.

resistive load, the cooling load is represented by an RL load, and there is no on-board power supply unit model.

Fig. 14 shows the comparison result during a 16% voltage sag event between the proposed model and the reference model. The simulation waveforms are all normalized into p.u. values, including the terminal voltage magnitude $V_{t,pu}$, the terminal active power and reactive power $P_{t,pu}, Q_{t,pu}$, and the single-phase ac voltage of the rack-level power supply $V_{ac\_PSU,pu}$. During the voltage sag disturbance, the data center transitions between normal mode (switch S_2 is ON, S_3 is OFF) and double conversion mode (switch S_2 is OFF, S_3 is ON). In both modes, S_1, S_4–S_7 remain ON, and S_8 remains OFF. In the proposed model, when a voltage sag occurs at $t = 2$ s, the aggregated cooling motor and power supply converters respond accordingly to maintain the same output power. After 500 ms, switch S_2 is disconnected and S_3 is turned ON so that the server loads are carried by the UPS. During the mode transition, the UPS switches from very light load to heavy server load, and distinct dips are captured in $P_{t,pu}$ and $V_{ac\_PSU,pu}$ at 2.5 s (see Fig. 14). Server loads are supported by the UPS regulated power until 0.25 s after the sag ends, and the UPS drops out at $t = 3.25$ s. Since the server power supply and cooling load are simplified as constant RL load, the reference model presents decreased power during 2–2.5 s, and the dynamic response deviates from the proposed model. Therefore, the proposed data center model is more complete and accurate to represent the data center load characteristics.

IV. DEVELOPMENT OF AN ALL-IN-ONE LOAD DATA CENTER POWER EMULATOR

In order to improve the evaluation of the grid dynamic performance, a data center power emulator is developed based on the proposed data center model. The whole data center power system is emulated in local VSIs in the CURENT HTB [5], serving as an all-in-one load.

A. Model Digitization

Since the data center power emulator is implemented in the HTB VSI, a digitized model with discrete-time equations is proposed to embed the data center dynamic model into the VSI digital signal processor (DSP). All PI controllers of power converters are expressed in the form of

$$
\begin{cases}
e[x] = Y_{ref}^{pu}[x] - \bar{y}^{pu}[x-1] \\
\bar{s}_c^{pu}[x] = k_p e[x] + \sum_0^x k_i e[x] T_s
\end{cases}
\tag{4}
$$

where $\bar{y}^{pu}$ is the controlled parameter, $e[x]$ is the error from the reference value $Y_{ref}^{pu}[x]$, k_p, k_i are PI parameters, and $\bar{s}_c^{pu}[x]$ is the control signal.

1) Digitized UPS Model: The UPS VSI model in discrete-time equation is

$$
\begin{cases}
\overrightarrow{\bar{i}_{dq,vsi}}[x] = \dfrac{T_s}{L_{vsi}} \bar{v}_{dc,vsi}[x-1] \overrightarrow{d_{dq,vsi}}[x] - \dfrac{T_s}{L_{vsi}} \overrightarrow{\bar{v}_{dq,vsi}}[x-1] \\
\qquad + \begin{bmatrix} 1 & \omega T_s \\ -\omega T_s & 1 \end{bmatrix} \overrightarrow{\bar{i}_{dq,vsi}}[x-1] \\
\overrightarrow{\bar{v}_{dq,vsi}}[x] = \dfrac{T_s}{C_{vsi}} \overrightarrow{\bar{i}_{dq,vsi}}[x-1] - \dfrac{T_s}{C_{vsi}} \overrightarrow{\bar{i}_{load\_dq,vsi}}[x-1] \\
\qquad + \begin{bmatrix} 1 & \omega T_s \\ -\omega T_s & 1 \end{bmatrix} \overrightarrow{\bar{v}_{dq,vsi}}[x-1] \\
\bar{i}_{dc,vsi}[x] = \overrightarrow{d_{dq,vsi}}^T[x] \overrightarrow{\bar{i}_{dq,vsi}}[x-1]
\end{cases}
\tag{5}
$$

where $\overrightarrow{d_{dq,vsi}}[x]$ is from the digitized current-loop controller.

The UPS rectifier model in discrete-time equation is

$$
\begin{cases}
\bar{i}_{L,rec}[x] = \bar{i}_{c,rec}^{[}x] I_{B,ups} \\
\bar{v}_{diode}[x] = \max\{\bar{v}_{ab,rec}[x], \bar{v}_{ac,rec}[x], \dots, \bar{v}_{cb,rec}[x]\} \\
\bar{v}_{dc,ups}[x] = \dfrac{T_s}{C_{dc,ups}} \left(\dfrac{\bar{v}_{diode}[x] \bar{i}_{L,rec}[x]}{\bar{v}_{dc,ups}[x-1]} - \bar{i}_{load,rec}[x-1] \right) \\
\qquad + \bar{v}_{dc,ups}[x-1]
\end{cases}
\tag{6}
$$

$$
\begin{cases}
if \; \bar{v}_{diode}[x] = \bar{v}_{ab,rec}[x] \\
\bar{i}_{a,rec}[x] = \bar{i}_{L,rec}[x], \bar{i}_{b,rec}[x] = -\bar{i}_{L,rec}[x], \bar{i}_{c,rec}[x] = 0 \\
if \; \bar{v}_{diode}[x] = \bar{v}_{ac,rec}[x] \\
\bar{i}_{a,rec}[x] = \bar{i}_{L,rec}[x], \bar{i}_{b,rec}[x] = 0, \bar{i}_{c,rec}[x] = -\bar{i}_{L,rec}[x] \\
if \; \bar{v}_{diode}[x] = \bar{v}_{bc,rec}[x] \\
\bar{i}_{a,rec}[x] = 0, \bar{i}_{b,rec}[x] = \bar{i}_{L,rec}[x], \bar{i}_{c,rec}[x] = -\bar{i}_{L,rec}[x] \\
if \; \bar{v}_{diode}[x] = \bar{v}_{ba,rec}[x] \\
\bar{i}_{a,rec}[x] = -\bar{i}_{L,rec}[x], \bar{i}_{b,rec}[x] = \bar{i}_{L,rec}[x], \bar{i}_{c,rec}[x] = 0 \\
if \; \bar{v}_{diode}[x] = \bar{v}_{ca,rec}[x] \\
\bar{i}_{a,rec}[x] = -\bar{i}_{L,rec}[x], \bar{i}_{b,rec}[x] = 0, \bar{i}_{c,rec}[x] = \bar{i}_{L,rec}[x] \\
if \; \bar{v}_{diode}[x] = \bar{v}_{cb,rec}[x] \\
\bar{i}_{a,rec}[x] = 0, \bar{i}_{b,rec}[x] = -\bar{i}_{L,rec}[x], \bar{i}_{c,rec}[x] = \bar{i}_{L,rec}[x]
\end{cases}
\tag{7}
$$

where $\bar{i}_{c,rec}^{pu}[x]$ is from the digitized voltage-loop controller and $I_{B,ups}$ is the UPS base current value used in the p.u. system.

The UPS dc–dc converter model in discrete-time equation is

$$
\begin{cases}
\bar{i}_{batt}[x] = -\dfrac{T_s}{L_{dc,dc}} (1 - d_{dcdc}[x]) \bar{v}_{dc}[x-1] \\
\qquad + \dfrac{T_s}{L_{dc,dc}} \bar{v}_{batt}[x-1] + \bar{i}_{batt}[x-1] \\
\bar{i}_{dc,dc}[x] = (1 - d_{dcdc}[x]) \bar{i}_{batt}[x]
\end{cases}
\tag{8}
$$

where $d_{dcdc}[x]$ is from the digitized current-loop controller. The discrete Li-ion battery model developed in [23] is adopted.

Because of the multiple operation modes, modeling of the UPS dc bus voltage and load current changes with mode transition, and the resulting discrete-time equations are as follows. In eco normal mode and double conversion mode

$$
\begin{cases}
\bar{v}_{dc,ups}[x] = \dfrac{T_s}{C_{dc,ups}} (\bar{i}_{dc,rec}[x] + \bar{i}_{dc,dc}[x] - \bar{i}_{dc,vsi}[x]) \\
\qquad + \bar{v}_{dc,ups}[x-1] \\
\bar{i}_{load,rec}[x] = \bar{i}_{dc,vsi}[x] - \bar{i}_{dc,dc}[x] \\
\overrightarrow{\bar{i}_{load\_dq,vsi}}[x] = \dfrac{\overrightarrow{\bar{v}_{dq,vsi}}[x]}{R_{load,eco}} \text{(normal mode)} \\
\qquad = \dfrac{N_{psu}}{3} \overrightarrow{\bar{i}_{in\_dq,pfc}}[x] \text{(double conversion mode)}.
\end{cases}
\tag{9}
$$

In battery mode

$$
\begin{cases}
\bar{v}_{dc,ups}[x] = \dfrac{T_s}{C_{dc,ups}} (\bar{i}_{dc,dc}[x] - \bar{i}_{dc,vsi}[x]) + \bar{v}_{dc,ups}[x-1] \\
\bar{i}_{load,rec}[x] = 0 \\
\overrightarrow{\bar{i}_{load\_dq,vsi}}[x] = \dfrac{N_{psu}}{3} \overrightarrow{\bar{i}_{in\_dq,pfc}}[x] + \overrightarrow{\bar{i}_{dq,vfd}}[x]
\end{cases}
\tag{10}
$$

where N_{psu} is the total number of PSUs.

2) Digitized PSU PFC Model:

$$
\begin{cases}
\bar{v}_{diode,pfc}[x] = |\bar{v}_{in,pfc}[x]| \\
\bar{i}_{Lb}[x] = -\dfrac{T_s}{L_b} (1 - d_{pfc}[x]) \bar{v}_{dc,psu}[x-1] \\
\qquad + \dfrac{T_s}{L_b} \bar{v}_{diode,pfc}[x] + \bar{i}_{Lb}[x-1] \\
\bar{v}_{dc,psu}[x] = \dfrac{T_s}{C_{dc,psu}} (1 - d_{pfc}[x]) \bar{i}_{Lb}[x] \\
\qquad - \dfrac{T_s}{C_{dc,psu}} \bar{i}_{load,pfc}[x-1] + \bar{v}_{dc,psu}[x-1] \\
\bar{i}_{load,pfc} = \dfrac{N_{s,psu} P_{server}[x]}{\bar{v}_{dc,psu}[x]}
\end{cases}
\tag{11}
$$

where $d_{pfc}[x]$ is from the digitized current-loop controller, and $N_{s,psu}$ is the number of servers supplied by one PSU.

3) Digitized VFD Model: The rectifier average model in discrete-time equations is

$$
\begin{cases}
\overrightarrow{\bar{i}_{dq,vfd}}[x] = -\dfrac{T_s}{L_{vfd}} \bar{v}_{dc,vfd}[x-1] \overrightarrow{d_{dq,vfd}}[x] \\
\qquad + \dfrac{T_s}{L_{vfd}} \overrightarrow{\bar{v}_{dq,vfd}}[x-1] + \begin{bmatrix} 1 & \omega T_s \\ -\omega T_s & 1 \end{bmatrix} \overrightarrow{\bar{i}_{dq,vfd}}[x-1] \\
\bar{v}_{dc,vfd}[x] = \dfrac{T_s}{C_{dc,vfd}} \overrightarrow{d_{dq,vfd}}^T[x] \overrightarrow{\bar{i}_{dq,vfd}}[x-1] \\
\qquad - \dfrac{T_s}{C_{dc,vfd}} \bar{i}_{dc,vfd}[x-1] + \bar{v}_{dc,vfd}[x-1]
\end{cases}
\tag{12}
$$

where $\overrightarrow{d_{dq,vfd}}[x]$ is from the digitized current-loop controller.

Based on the constant V/Hz control, the VSI output voltage $v_{dq\_vsi,vfd}$ is proportional to the reference rotation angular frequency $\omega_{r\_ref,vfd}$ that is determined by the required air flow rate.

$$\begin{cases} v_{d\_vsi,vfd}[x] = 0 \\ v_{q\_vsi,vfd}[x] = \omega_{m\_ref}[x]\frac{PV_b}{2\omega_b}. \end{cases} \quad (13)$$

For the induction motor representing the cooling tower, chiller, and water pumps, the discrete model developed in [21] is employed.

B. Model Simplification

An all-in-one load power emulator was implemented in a few local VSIs in the CURENT HTB, so that the emulator can be flexibly installed or modified in various bus terminals of the power grid emulation platform. To reduce the computation cost and implement the complicated data center system model into an all-in-one load emulator, reasonable simplification of the digitized data center model is required, but the simplified model should also maintain modeling accuracy. Recalling the dual-loop control used in the data center UPS VSI, UPS dc–dc converter, the PSU PFC converter, and the CRAH VFD front-end rectifier, the inner current loops have much higher bandwidth than the grid line frequency and can be viewed as ideal controls. Therefore, the digitized model is simplified by neglecting the fast current loop and replacing the current with the current reference generated from the voltage loop.

The UPS VSI current loop model is simplified as

$$\begin{cases} \overrightarrow{i_{dq,vsi}} = \overrightarrow{i^{pu}_{dqref,vsi}}I_{B,ups} \\ \overrightarrow{d_{dq,vsi}}[x] = \frac{\overrightarrow{v_{dq,vsi}}[x-1]}{\overline{v}_{dc,vsi}[x-1]} - \\ \frac{L_{vsi}}{T_s\overline{v}_{dc,vsi}[x-1]}\left(\begin{bmatrix} 1 & \omega T_s \\ -\omega T_s & 1 \end{bmatrix}\overrightarrow{i_{dq,vsi}}[x-1] - \overrightarrow{i_{dq,vsi}}[x]\right). \end{cases} \quad (14)$$

The UPS dc–dc converter current loop model is simplified as

$$\begin{cases} \overline{i}_{batt}[x] = \overline{i}^{pu}_{batt\_ref}[x] \\ d_{dcdc}[x] = 1 - \frac{\overline{v}_{batt}[x-1]}{\overline{v}_{dc}[x-1]}. \end{cases} \quad (15)$$

The PSU PFC current loop model is simplified as

$$\begin{cases} \overline{i}_{Lb}[x] = \overline{i}^{pu}_{Lb\_ref}[x] \\ d_{pfc}[x] = 1 - \frac{\overline{v}_{diode,pfc}[x]}{\overline{v}_{dc,psu}[x-1]}. \end{cases} \quad (16)$$

The VFD rectifier current loop model is simplified as

$$\begin{cases} \overrightarrow{i_{dq,vfd}}[x] = \overline{i}^{pu}_{qref,vfd}[x] \\ \overrightarrow{d_{dq,vfd}}[x] = \frac{\overrightarrow{v_{dq,vfd}}[x-1]}{\overline{v}_{dc,vfd}[x-1]} + \\ \frac{L_{vfd}}{T_s\overline{v}_{dc,vfd}[x-1]}\left(\begin{bmatrix} 1 & \omega T_s \\ -\omega T_s & 1 \end{bmatrix}\overrightarrow{i_{dq,vfd}}[x-1] - \overrightarrow{i_{dq,vfd}}[x]\right). \end{cases} \quad (17)$$

Fig. 15 shows the comparison result during a voltage sag event of the detailed data center dynamic model and the simplified digitized model, where the data center operates from normal eco mode to double conversion mode. Dynamic performance
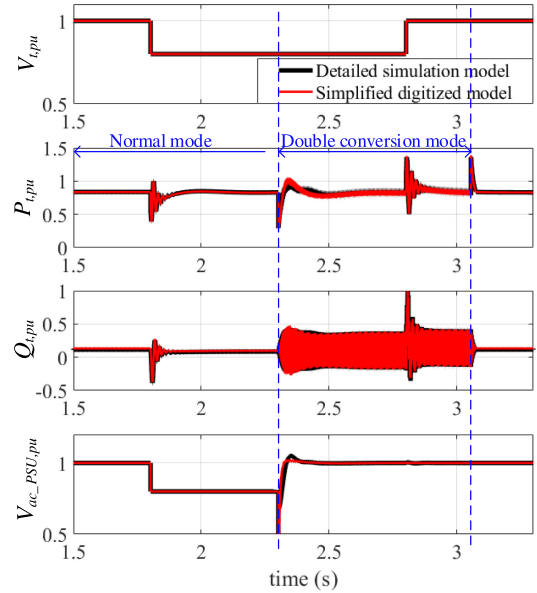

Fig. 15. Comparison of the detailed data center dynamic model in simulation and the simplified digitized model with sampling frequency at 5kHz during a 20% voltage sag event for 1 s.

TABLE IV
SPECIFICATIONS OF THE VSIs UNDER TEST

Parameters	Values
DC link voltage	200 V
Switching frequency	10 kHz
Power rating	2 kW
Line impedance	1.8 mH
Base power under test	500 W

predicted by the simplified digitized model is consistent with the detailed model and is accurate enough to implement the all-in-one data center power emulator.

C. Hardware Implementation

The emulator is implemented on the CURENT HTB, which is a multiconverter-based real-time real-power testing platform and can be flexibly emulated by programming the interconnected three-phase VSIs [5]. A local network consisting of three VSIs in one cabinet is used for the data center emulator verification, as illustrated in Fig. 16. VSI-1 is implemented as a generator emulator to represent the grid power source that is connected to the emulator through line impedance. The data center is emulated by two VSIs, where VSI-2 is embedded with models of UPS, PDUs, PSUs, and CRAH; and VSI-3 is installed with the aggregated induction motor model for cooling tower, chiller, and water pumps. In each of the load VSIs, the conditioning function, the data center model, and the VSI inner current loop are embedded in one DSP. The conditioned terminal voltage $v_{t,dq}$ and frequency is sent to the load model to generate the reference current i_{t,dq_ref}, which is sent to the inner current loop to control the VSI and generate the required terminal current. In this way, the VSIs are configured to emulate the data center load characteristics. Table IV presents the specifications of the VSIs under test.
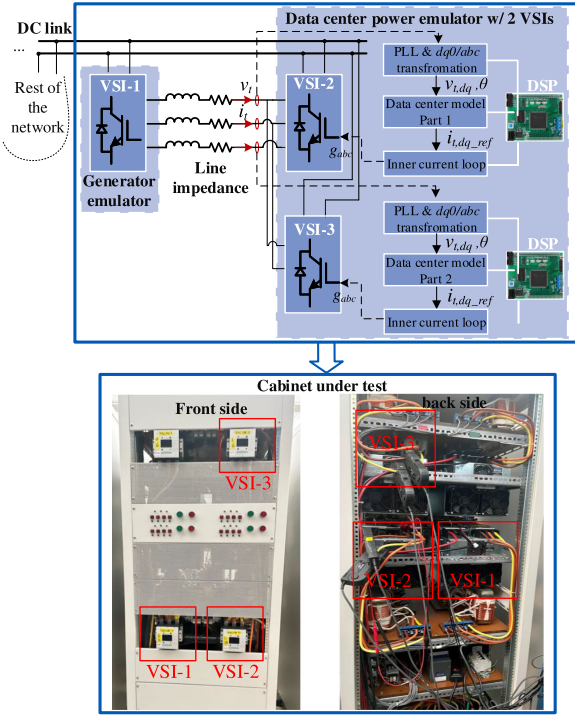
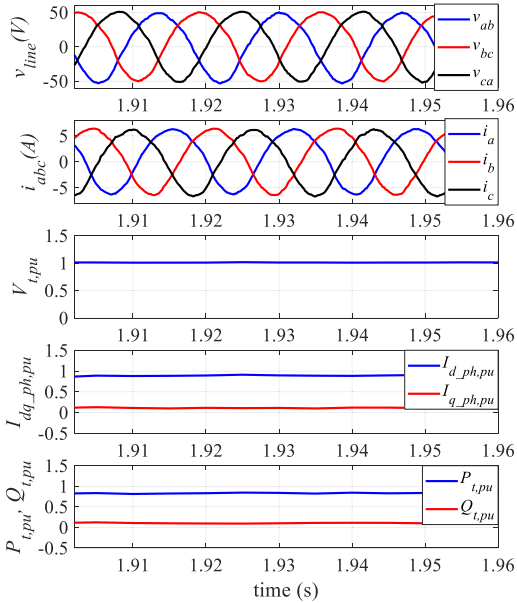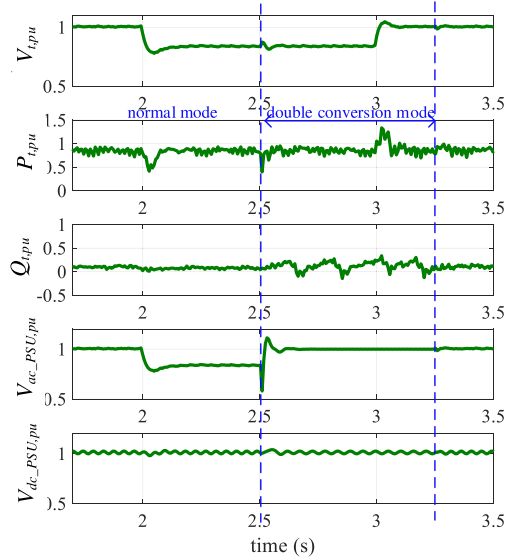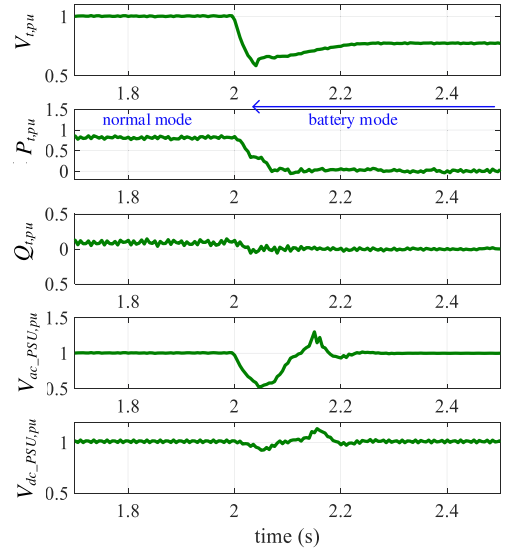Fig. 16. Experimental setup for the data center emulator verification.

Fig. 17. Experimental waveforms at steady state with 100% server utilization.

Fig. 18. Experimental emulation results of the data center power system during voltage sag events. (a) Mode transition between normal eco mode and double conversion mode with 16% terminal voltage sag for 1 s. (b) Mode transition between normal eco mode and battery mode with > 30% terminal voltage sag.

V. EXPERIMENTAL VERIFICATION

The data center power emulator is first validated at steady state with normal input voltage. Fig. 17 shows the tested waveforms, including the three-phase line-to-line voltages v_{line}, three-phase currents i_{abc}, normalized terminal voltage magnitude $V_{t,pu}$, normalized currents in dq axis $I_{dq\_ph,pu}$, and normalized active and reactive power $P_{t,pu}$, $Q_{t,pu}$. At full load with 100% server utilization, the measured $P_{t,pu} = 0.837$, $Q_{t,pu} = 0.11$, and PF = 0.99.

A. Experimental Emulation of Voltage Sag Events

Voltage sag is one of the most common grid disturbances, which are demonstrated to emulate the dynamic response of the data center load. Fig. 18 shows the experimental results during two voltage sag events. When a 16% voltage sag occurs [see Fig. 18(a)], the data center changes operation from normal eco mode to double conversion mode after 500ms at $t = 2.5$s. At the same time, the UPS switches from what was a very light load to now heavy server loads, leading to a transient response with an abrupt power variation and slight $V_{t,pu}$ fluctuation. At both the beginning and end of the voltage sag, the data center performs transient power change due to the sudden voltage variation.
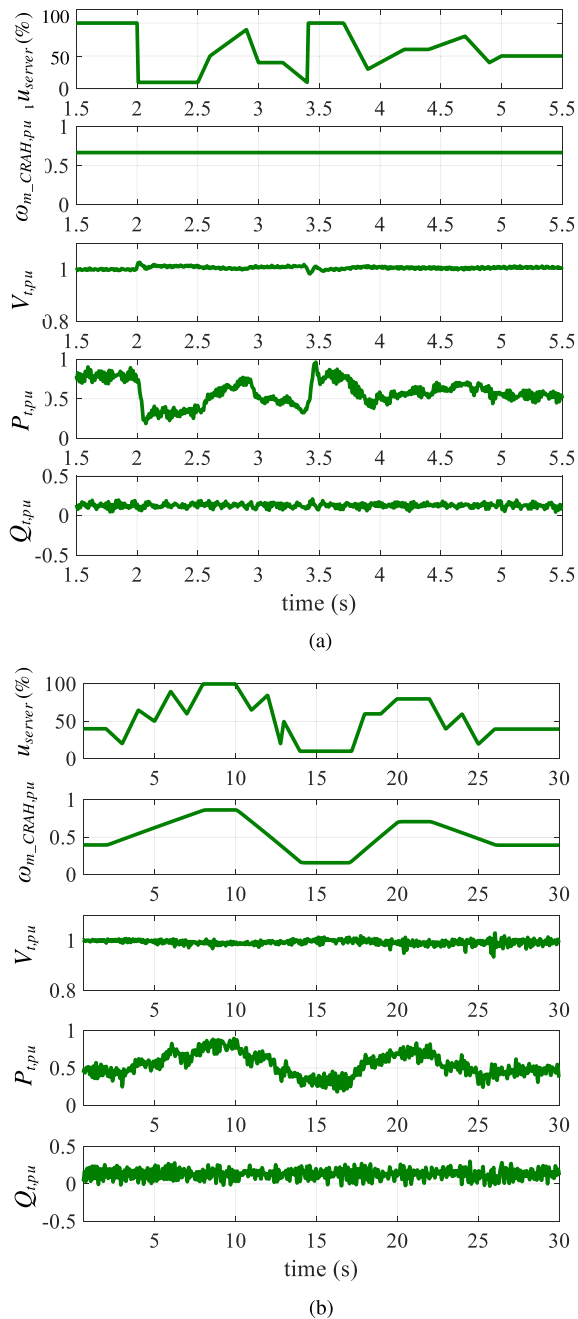
Fig. 19. Experimental emulation results of the data center power system during load variations. (a) Case 1: operation waveforms under load variation for 3 s. (b) Case 2: operation waveforms under load variation for 30 s.

Fig. 18(b) shows a more severe voltage sag with voltage drop $> 30\%$. To protect PSUs and maintain normal server operation, data center load is disconnected from the grid 20ms after the sag occurs, and the UPS battery switches in to support the load. Consequently, $P_{t,\text{pu}}$ and $Q_{t,\text{pu}}$ drop to zero after the data center power system is disconnected from the grid during the battery mode. With the line impedance (1.8mH) used in the experimental setup, V_t oscillates sometime after the transition to battery mode and increases slightly from its low point immediately. In both power interruptions, the PSU dc voltage is held at a high

level to maintain the normal operation of server loads. Dynamic performance during mode transition between double-conversion mode and battery mode can also be emulated by the data center emulator.

B. Experimental Emulation of Server Load Variations

Transient response at grid point of common coupling during server load variations is investigated. Two load profiles are performed in the emulator under the assumption that server tasks are evenly distributed. In case 1, the server load behaves with extreme variations in a short time (i.e., 3 s), and the server room air flow does not change accordingly due to slower thermal dynamics. In case 2, the server load changes in a longer time (i.e., 30 s), and CRAH motor adjusts rotation speed accordingly to meet the server room air flow demand.

Fig. 19 presents the experimental results during server load variations. The data center power consumption generally follows the server loading, but has significant load variations ranging from 0.18 to 0.96 p.u. in case 1 and 0.25 to 0.91 p.u. in case 2. Such power dynamic response is more obvious during the period with higher u_{server} change rate, and results in terminal voltage fluctuations of the regional grid.

VI. CONCLUSION

To investigate data centers' load characteristic and evaluate the grid dynamic performance, this article proposed a dynamic data center model, and a data center power load emulator based on CURENT HTB was also developed.

The data center model was complete, containing the power supply system, cooling system, detailed server load, and cooling load. Compared with the conventional model, the proposed model had detailed modeling of power converters and control dynamics. Coherent server load and cooling load ensured realistic load model of the data center. Also, the proposed generalized model allowed the prediction of data center dynamic power performance in different operation modes. Therefore, the proposed data center dynamic power model led to a more realistic and accurate prediction of data center load characteristics. The data center dynamic model can also be used to study some internal operations, such as investigating the UPS battery SOC limit for safe power transition and the power supply peak current for protection.

The developed data center power emulator was verified experimentally in a regional power network in the HTB, and transient characteristics during voltage sag events and server load variations were demonstrated. Compared with existing emulators, the proposed data center power emulator is capable of assessing dynamic power performance. With model digitization and simplification, the emulator serves as an all-in-one load in the CURENT HTB, and it can be flexibly installed in different bus terminals to perform various local or large-scale power system experiments. Therefore, the data center emulator provides an effective and easy-to-use alternative to physical data center prototype for power system study.

APPENDIX A
COOLING SYSTEM POWER LOAD CALCULATION

1) Server Fan Power Consumption:

$$P_{\text{fan,server}} = P_{\text{rated,fan}} \frac{f_{\text{air,server}}^3}{f_{\text{0fan,server}}^3} (\text{W}) \qquad (18)$$

where $P_{\text{rated,fan}}$ is the fan power rating, $f_{\text{0fan,server}}$ is the nominal air flow rate, and $f_{\text{air,server}}$ is the required air flow per server, which is defined by the power of the server power supply, including the server load and power supply loss

$$f_{\text{air,server}} = \frac{P_{\text{server}}}{\eta_{\text{server}} \triangle T_{\text{air,server}} \rho_{\text{air}} c_{\text{air}}} (\text{m}^3/\text{s}) \qquad (19)$$

where η_{server} represents the efficiency of the server power supply, ρ_{air} is the air density, c_{air} is the air heat capacity, and $\triangle T_{\text{air,server}}$ is the allowable server temperature range.

2) CRAH Power Load:

$$P_{\text{load,CRAH}} = P_{\text{rated,CRAH}} \frac{f_{\text{air,room}}^3}{f_{\text{0fan,CRAH}}^3} (\text{W}) \qquad (20)$$

where $P_{\text{rated,CRAH}}$ is the CRAH rated output power, $f_{\text{0fan,CRAH}}$ is the nominal fan speed of the CRAH motor, $f_{\text{air,room}}$ is the total air flow rate in the server room.

$$f_{\text{air,room}} = (1 - k) N_{\text{rack}} N_{\text{server}} f_{\text{air,server}} (\text{m}^3/\text{s}) \qquad (21)$$

where k serves as the recirculation index.

3) Chiller Power Load:

$$P_{\text{load,chiller}} = \frac{Q_{\text{chiller}}}{\text{COP}_{\text{chiller}}} (\text{W}) \qquad (22)$$

Q_{chiller} is the chiller thermal load, which is calculated as

$$Q_{\text{chiller}} = (1 - k) Q_{\text{CRAH}} = 1158.2 f_{\text{air,room}} \triangle T_{\text{air, CRAH}} (\text{W}) \qquad (23)$$

where $\triangle T_{\text{air, CRAH}}$ is the temperature difference between the CRAH hot air and the cold air. The chiller COP is estimated based on the water temperature flowing through the chiller

$$\text{COP}_{\text{chiller}} = \frac{T_{w\text{cold,chiller}}}{\triangle T_{w,\text{chiller}}} = \frac{T_{w\text{cold,chiller}} f_{w,\text{chiller}} \rho_w c_w}{Q_{\text{chiller}}} \qquad (24)$$

where $T_{w\text{cold,chiller}}$ is the chiller cold water temperature, $\triangle T_{w,\text{chiller}}$ is the temperature difference between the cold water and the hot water, $f_{w,\text{chiller}}$ is the chiller water flow rate, ρ_w is the water density, and c_w is the water heat capacity.

4) Cooling Tower Power Load:

$$P_{\text{load,CT}} = \frac{Q_{\text{CT}}}{\text{COP}_{\text{CT}}} (\text{W}). \qquad (25)$$

The cooling tower is responsible for cooling the hot water from the chiller, and removing the heat from the UPS, chiller, CRAH, and other power components. Hence, the cooling tower thermal load is estimated as

$$Q_{\text{CT}} = Q_{\text{chiller}} + P_{\text{loss, UPS}} + P_{\text{loss,CRAH}} + P_{\text{loss,chiller}} (\text{W}). \qquad (26)$$

And the COP of cooling tower is determined with

$$\text{COP}_{\text{CT}} = \frac{T_{w\text{cold,CT}}}{\triangle T_{w,\text{CT}}} = \frac{T_{w\text{cold,CT}} f_{w,\text{CT}} \rho_w c_w}{Q_{\text{CT}}} \qquad (27)$$

where $T_{w\text{cold,CT}}$ is the cold water temperature in the cooling tower, $\triangle T_{w,\text{CT}}$ is the cooling tower water temperature difference between the cold water and the hot water, $f_{w,\text{CT}}$ is the cooling tower water flow rate.

5) Water Pump Power Load:

$$P_{\text{load, pump1}} = 2.79 \times 10^5 f_{w,\text{chiller}} \triangle T_{w,\text{chiller}} (\text{W}) \qquad (28)$$

$$P_{\text{load, pump2}} = 2.79 \times 10^5 f_{w,\text{CT}} \triangle T_{w,\text{CT}} (\text{W}). \qquad (29)$$

REFERENCES

[1] P. T. Krein, "Data center challenges and their power electronics," *CPSS Trans. Power Electron. Appl.*, vol. 2, no. 1, pp. 39–46, 2017.

[2] S. Masanet and L. Smith, "Global data center energy use: Distribution, composition, and near-term outlook," Northwestern University: Evanston, IL, USA, 2018.

[3] R. Rahmani, I. Moser, and M. Seyedmahmoudian, "A complete model for modular simulation of data centre power load," 2018, *arXiv:1804.00703*.

[4] ANSI/BICSI 002, *Data Center Design and Implementation Best Practices*, 2019.

[5] J. Wang *et al.*, "Static and dynamic power system load emulation in a converter-based reconfigurable power grid emulator," *IEEE Trans. Power Electron.*, vol. 31, no. 4, pp. 3239–3251, Apr. 2016.

[6] D. Mao, K. Potty, and J. Wang, "The impact of power-electronics-based load dynamics on large-disturbance voltage stability," in *Proc. IEEE Power Energy Soc. Gen. Meeting*, 2018, pp. 1–5.

[7] J. Spitaels, "Dynamic power variations in data centers and network rooms," *Amer. Power Convers.*, White Paper 43, 2005.

[8] Z. Zhou *et al.*, "Fine-grained energy consumption model of servers based on task characteristics in cloud data center," *IEEE Access*, vol. 6, pp. 27080–27090, 2018.

[9] R. Das, J. O. Kephart, J. Lenchner, and H. Hamann, "Utility-function-driven energy-efficient cooling in data centers," in *Proc. 7th Int. Conf. Autonomic Comput.*, 2010, pp. 61–70.

[10] G. Zhabelova, M. Vesterlund, S. Eschmann, Y. Berezovskaya, V. Vyatkin, and D. Flieller, "A comprehensive model of data center: From CPU to cooling tower," *IEEE Access*, vol. 6, pp. 61254–61266, 2018.

[11] S. Yeo and H.-H. S. Lee, "SimWare: A holistic warehouse-scale computer simulator," *Computer*, vol. 45, no. 9, pp. 48–55, 2012.

[12] M. Tighe, G. Keller, M. Bauer, and H. Lutfiyya, "DCSim: A data centre simulation tool for evaluating dynamic virtualized resource management," in *Proc. 8th Int. Conf. Netw. Serv. Manage. Workshop Syst. Virtualization Manage.*, 2012, pp. 385–392.

[13] G. Zhabelova, A. Yavarian, and V. Vyatkin, "Data center power dynamics within the settings of regional power grid," in *Proc. IEEE 20th Conf. Emerg. Technol. Factory Automat.*, 2015, pp. 1–5.

[14] B. R. Shrestha, U. Tamrakar, T. M. Hansen, B. P. Bhattarai, S. James, and R. Tonkoski, "Efficiency and reliability analyses of AC and 380 V DC distribution in data centers," *IEEE Access*, vol. 6, pp. 63305–63315, 2018.

[15] L. Yang *et al.*, "Three-phase power converter-based real-time synchronous generator emulation," *IEEE Trans. Power Electron.*, vol. 32, no. 2, pp. 1651–1665, Feb. 2017.

[16] S. Suryanarayanan, W. Ren, M. Steurer, F. Ribeiro, and G. Heydt, "A real-time controller concept demonstration for distributed generation interconnection," in *Proc. IEEE Power Eng. Soc. Gen. Meeting*, 2006, pp. 3–6.

[17] R. H. Lasseter *et al.*, "CERTS microgrid laboratory test bed," *IEEE Trans. Power Del.*, vol. 26, no. 1, pp. 325–332, Jan. 2011.

[18] J. Mahseredjian, V. Dinavahi, and J. A. Martinez, "Simulation tools for electromagnetic transients in power systems: Overview and challenges," *IEEE Trans. Power Del.*, vol. 24, no. 3, pp. 1657–1669, Jul. 2009.

[19] S. Grubic, B. Amlang, W. Schumacher, and A. Wenzel, "A high-performance electronic hardware-in-the-loop drive-load simulation using a linear inverter," *IEEE Trans. Ind. Electron.*, vol. 57, no. 4, pp. 1208–1216, Apr. 2010.

[20] L. M. Tolbert *et al.*, "Reconfigurable real-time power grid emulator for systems with high penetration of renewables," *IEEE Open Access J. Power Energy*, vol. 7, pp. 489–500, Oct. 2020.

[21] J. Wang, Y. Ma, L. Yang, L. M. Tolbert, and F. Wang, "Power converter-based three-phase induction motor load emulator," in *Proc. 28th IEEE Appl. Power Electron. Conf. Expo.*, 2013, pp. 3270–3274.

[22] S. Wang, H. Li, J. Wang, Y. Ma, F. Wang, and L. M. Tolbert, "A power converter based real-time air-conditioner motor emulator," in *Proc. IEEE Appl. Power Electron. Conf. Expo.*, 2020, pp. 70–76.

[23] J. D. Boles, Y. Ma, J. Wang, D. Osipov, L. M. Tolbert, and F. Wang, "Converter-based emulation of battery energy storage systems (BESS) for grid applications," *IEEE Trans. Ind. Appl.*, vol. 55, no. 4, pp. 4020–4032, Jul./Aug. 2019.

[24] J. Sun, S. Wang, J. Wang, and L. M. Tolbert, "Development of a converter-based data center power emulator," in *Proc. IEEE Appl. Power Electron. Conf. Expo.*, 2021, pp. 126–133.

[25] Eaton, "Eaton 93 M UPS: 480 V three-wire – 400 kW frame installation and operation manual." Accessed: Dec 21, 2018. [Online]. Available: https://www.eaton.com/us/en-us/catalog/backup-power-ups-surge-it-power-distribution/eaton-93pm-ups.html

[26] Delta Electronics, "Standard power supplies," Accessed: Oct, 2018. [Online]. Available: https://www.avnet.com/wps/wcm/connect/onesite/7773ed99-8890-4a6c-b2a0-e01c0b56caed/Delta-standard-power-supplies-catalog-october-2018.pdf

[27] B. Yang, F. C. Lee, A. Zhang, and G. Huang, "LLC resonant converter for front end DC/DC conversion," in *Proc. 17th IEEE Appl. Power Electron. Conf. Expo.*, 2002, pp. 1108–1112.

[28] *Intel Corporation*, "Voltage regulator-down (VRD) 11.0, processor power delivery design guidelines." Accessed: Nov. 2006. [Online]. Available: https://www.intel.com.au/content/dam/doc/design-guide/voltage-regulator-down-11-0-processor-power-delivery-guide.pdf

[29] A. Emadi, A. Nasiri, and S. B. Bekiarov, *Uninterruptible Power Supplies and Active Filters*. Boca Raton, FL, USA: CRC Press, 2017.

[30] S. Hiti, "Modeling and control of three-phase PWM converters," Ph.D. dissertation, Dept. Elect. Eng., Virginia Tech, Blacksburg, VA, USA, 1995.

[31] R. Hidalgo-León and P. Jácome-Ruiz, "A survey on technologies to implement battery emulators based on DC/DC power converters," in *Proc. LACCEI Int. Multi-Conf. Eng., Educ., Technol.*, 2016, pp. 1–11.

[32] P. C. Krause, O. Wasynczuk, S. D. Sudhoff, and S. Pekarek, *Analysis of Electric Machinery and Drive Systems*, vol. 2. Hoboken, NJ, USA: Wiley Online Library, 2002.

[33] X. Liu, D. Teng, D. Wang, Q. Zhu, and Z. Liu, "Application of eco mode UPS in data center," in *Proc. IEEE Int. Telecommun. Energy Conf.*, 2017, pp. 30–34.

[34] Y. Joshi and P. Kumar, *Energy Efficient Thermal Management of Data Centers*. Berlin, Germany: Springer, 2012.

[35] *Information Technology Industry Council (ITIC)*, "ITI (CBEMA) curve application note," Accessed: Jan. 2022. [Online]. Available: http://www.itic.org

[36] K. Yao, Q. Meng, Y. Bo, and W. Hu, "Three-phase single-switch DCM boost PFC converter with optimum utilization control of switching cycles," *IEEE Trans. Ind. Electron.*, vol. 63, no. 1, pp. 60–70, Jan. 2016.

[37] T. Friedli, M. Hartmann, and J. W. Kolar, "The essence of three-phase PFC rectifier systems–Part I," *IEEE Trans. Power Electron.*, vol. 29, no. 2, pp. 543–560, Feb. 2014.

[38] O. Tremblay and L.-A. Dessaint, "Experimental validation of a battery dynamic model for EV applications," *World Electr. Veh. J.*, vol. 3, no. 2, pp. 289–298, 2009.

[39] X. He and J. W. Hodgson, "Modeling and simulation for hybrid electric vehicles," *IEEE Trans. Intell. Transp. Syst.*, vol. 3, no. 4, pp. 235–243, Dec. 2002.

[40] S. S. Shah, U. Raheja, and S. Bhattacharya, "Input impedance analyses of charge controlled and frequency controlled LLC resonant converter," in *Proc. IEEE Energy Convers. Congr. Expo.*, 2018, pp. 1–5.

[41] M. Dayarathna, Y. Wen, and R. Fan, "Data center energy consumption modeling: A survey," *IEEE Commun. Surv. Tut.*, vol. 18, no. 1, pp. 732–794, Jan./Mar. 2015.

[42] J. Wan, X. Gui, S. Kasahara, Y. Zhang, and R. Zhang, "Air flow measurement and management for improving cooling and energy efficiency in raised-floor data centers: A survey," *IEEE Access*, vol. 6, pp. 48867–48901, 2018.

[43] Intel Corporation, "Intel Xeon processor 5500 series-an intelligent approach to IT challenges," Accessed: Jan. 2021. [Online]. Available: https://download.intel.com/pressroom/kits/xeon/5500series.pdf

[44] Delta Electronics, "Server fan FHS-A9025S20," Accessed: Jan. 2021. [Online]. Available: https://www.delta-fan.com/Download/Spec/FHS-A9025S20.pdf

Jingjing Sun (Student Member, IEEE) received the B.S. degree in electrical engineering from Xi'an Jiaotong University, Xi'an, China, in 2016, and the M.S. degree in 2018 from the University of Tennessee, Knoxville, TN, USA, where she is currently working toward the Ph.D. degree in power electronics with CURENT.

Her research interests include applications of wide band-gap semiconductor devices, high-efficiency converter design, and data center power distribution system modeling and application.

Shuyao Wang (Member, IEEE) received the B.S. and M.S. degrees from North China Electric Power University, Beijing, China, in 2013 and 2016, respectively, and the Ph.D. degree from the University of Tennessee, Knoxville, TN, USA, in 2021, all in electrical engineering.

She is currently a Senior Applications Engineer with Monolithic Power System, Inc., San Jose, CA, USA. Her research interests include modular multilevel converters, HVdc transmission system, power grid ancillary services, and power electronics-based devices modeling.

Jingxin Wang (Member, IEEE) received the Ph.D. degree in power electronics and electrical drives from Shanghai Jiaotong University, Shanghai, China, in 2011.

He is a Research Associate with the Department of Electrical Engineering and Computer Science, the University of Tennessee, Knoxville, TN, USA. His research interests include high performance motor control, modular multilevel converter, power flow control, and renewable energy.

Leon M. Tolbert (Fellow, IEEE) received the bachelor's, M.S., and Ph.D. degrees in electrical engineering from the Georgia Institute of Technology, Atlanta, GA, USA, in 1989, 1991, and 1999, respectively.

He is currently a Chancellor's Professor and the Min H. Kao Professor with the Department of Electrical Engineering and Computer Science, University of Tennessee, Knoxville, TN, USA, where he is the Founding Member and Testbed Thrust Leader for the NSF/DOE Engineering Research Center, CURENT (Center for Ultra-wide-area Resilient Electric Energy Transmission Networks). He is also an Adjunct Participant with Oak Ridge National Laboratory, Oak Ridge, Tennessee, where he previously worked from 1991 to 2020. His research interests include the utility applications of power electronics, microgrids, electric vehicles, and wide bandgap semiconductors.

Dr. Tolbert was a recipient of the 2001 IEEE Industry Applications Society Outstanding Young Member Award, and Eight Prize Paper Awards from the IEEE Industry Applications Society, and IEEE Power Electronics Society. He was an Associate Editor for the IEEE Power Electronics Letters and IEEE TRANSACTIONS ON POWER ELECTRONICS from 2003 to 2013, and the Paper Review Chair for the Industry Power Converter Committee of the IEEE Industry Applications Society from 2014 to 2017. He is currently the Academic Deputy Editor-in-Chief for the *IEEE Power Electronics Magazine* (2021–2023).